Chapter 14
Common-Coil Nb$_3$Sn Dipole Program at BNL

Ramesh Gupta

Abstract This chapter summarizes the common-coil dipole research and development program at the Brookhaven National Laboratory (BNL). The program goals included: (a) the development of accelerator-quality dipoles based on the common-coil design concept; (b) the demonstration of "react-and-wind" technology for high field collider dipole magnets; and (c) the development and demonstration of a novel background field test facility with a large open space.

14.1 Introduction

The common-coil design concept (Gupta 1997) is a conductor-friendly design, based on a simple coil geometry with large bend radii, and is particularly suitable for brittle superconductors. The common-coil geometry is considered to be technically attractive for high field magnets as it puts lower strain on the conductors with smaller support structures as compared to other designs. The common-coil design is also expected to produce lower cost magnets in large volume in industry since it allows the use of less expensive production techniques (because of the simpler geometry), since the number of coils required is halved (as the same coils are shared between two apertures), and since it has reduced structural requirements.

Several magnets based on the common-coil dipole designs had earlier been proposed for the Very Large Hadron Collider (VLHC) in the USA (Fermilab 2001). The common-coil design has also been used in the present proposal for a Super proton–proton Collider in China (Wang et al. 2016), and is one of the design options under consideration for the proposed Future Circular Collider (Tommasini et al. 2017) at the European Organization for Nuclear Research (CERN). The basic design concept has been extensively studied (Gupta et al. 1999, 2007; Ambrosio et al. 2000; Sabbi et al. 2000) and demonstrated at Brookhaven National Laboratory (BNL), Fermi National Accelerator Laboratory (FNAL) and Lawrence Berkeley National Laboratory (LBNL) with a series of magnets (see this part of this book).

R. Gupta (✉)
BNL (Brookhaven National Laboratory), Brookhaven, NY, USA
e-mail: gupta@bnl.gov

A similar configuration had also previously been proposed independently by Danby for low field dipoles (Danby et al. 1983).

BNL has developed, fabricated, and tested a successful common-coil dipole model called DCC017 based on the react-and-wind (R&W) technique. This work is described in detail in this chapter.

The common-coil design facilitates modular geometry, which is good for combining coils made with different types of conductors in both research and development (R&D) magnets and in large-scale production of hybrid magnets. The existing common-coil magnet DCC017 at BNL has created a unique lower cost and fast turnaround magnet test facility. This new type of test facility allows the testing of coils with a variety of parameters in a 10 T background field without disassembling the DCC017 magnet. Given the fast turn-around and lower cost, this R&D can be both "high risk, high reward" and "systematic," and is likely to introduce a new way of doing high field magnet R&D.

14.2   Common-Coil Dipole Design Concept

14.2.1   Design Concept

The common-coil magnet design (Gupta 1997) is a two-in-one (also known as twin) block design that is primarily based on flat racetrack coils that are shared between two apertures. The main coils are common to both apertures, hence the name "common-coil dipole design." A schematic of the common-coil design for the main coils is shown in Fig. 14.1. A set of coils are placed on the left- and right-hand sides of the two vertically arranged apertures to produce magnetic fields in opposite directions. The bending radius in the ends is much larger than that in a conventional dipole design, as it is determined by the separation between the two apertures rather than the size of the aperture itself.

Fig. 14.1 Main coils of the basic common-coil dipole design concept
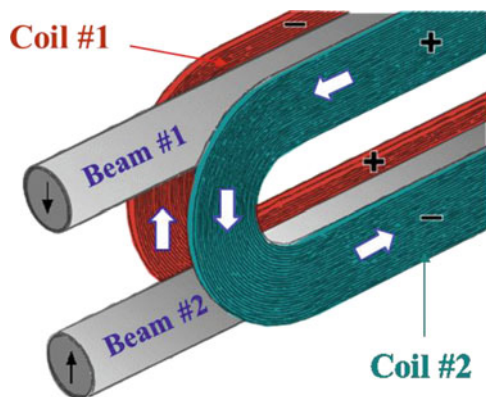
In addition to the main coils, pole coil blocks (see Sect. 14.3) are also needed to achieve the field quality required in accelerator magnets. These pole coil blocks may or may not have the same simple geometry as the main coils.

14.2.2 Common-Coil Mechanics

For very high field magnets, the magnet mechanics is a key component that determines the technical performance and cost of the magnet. In this respect, the common-coil geometry offers very different mechanics to maintain the large horizontal forces: The individual coils move as a whole, which minimizes the internal strain and stress on the conductor, particularly in the critical end region. Contrarily, in the cos-theta and conventional block designs, large horizontal forces create excessive stress/strain on the conductor in the end region. The BNL common-coil dipole tolerated about 0.2 mm displacement, which is significantly larger than the typical 0.1 mm allowed in cos-theta magnets. This larger allowed displacement, in principle, reduces the need for a large support structure, as long as the negative effects on the field quality are within acceptable limits.

Therefore, lower cost magnets due to a smaller structure and better performance due to less strain in the conductor could be expected. These features could be key for high field magnets where the magnet's structure is a major technical and cost issue. Moreover, the common-coil designs may also offer simpler stress management, if needed, since the layers of coils are stacked horizontally, and therefore planes for intercepting the Lorentz forces can be introduced.

14.2.3 Potential Advantages and Challenges of the Common-Coil Design

The common-coil geometry above described without auxiliary coils is expected to produce a lower cost, easier to manufacture, and technically attractive design for high field two-in-one dipoles. Several anticipated advantages of the common-coil design are listed below:

- Simple 2D coil geometry;
- Fewer coils (about half) as the same coils are common between the two apertures (two-in-one geometry for both iron and coils);
- Conductor-friendly with simpler ends and much larger bending radii, which are determined by the separation between the two apertures rather than the aperture itself;

- Additional technology option of R&W in addition to a wind-and-react (W&R) approach, especially for the main coils;
- Additional material options for insulation and coil material as, in the R&W approach, the coil does not go through a high-temperature reaction;
- More automated manufacturing options may be possible in large-scale production because of the simpler geometry;
- Lower internal strain on the conductor under Lorentz forces as the coils move as a unit;
- Savings from less support structure as much larger deflections are accepted.

The challenges with the common-coil design are listed below:

- Since the common-coil design is only applicable for two-in-one collider dipole geometry, it is a non-suitable design if only one aperture is needed.
- For two apertures, one needs about twice the amount of conductor as compared to that needed in single-aperture cos-theta or block dipole geometries, which could be a significant issue in R&D programs with limited budgets.
- The anticipated advantages of common design, listed above, are yet to be demonstrated.
- Pole coil blocks have to meet the field-quality requirements for accelerators, which require more complicated coil geometries.

Common-coil design offers additional advantages when used as the rapid turn-around magnet R&D test facility:

- A large open space can be incorporated between the apertures, where additional racetrack coils can be inserted and tested as an integral part of the magnet without requiring any disassembly (as in the BNL common-coil magnet DCC017);
- Flexible and modular design is offered with easier segmentation for hybrid high field dipoles using a variety of conductors (Nb_3Sn, Nb-Ti and for very high field high temperature superconductors (HTS));
- Minimum requirements for large, expensive tooling and labor, particularly during the R&D phase, are required;
- Efficient and rapid turn-around magnet R&D due to simpler and modular design might be possible.

14.3   Accelerator-Quality Common-Coil Dipole

Despite the early promise and success of the common-coil dipole design, further development stopped, not for technical reasons, but because of changing US Department of Energy program needs. Subsequent magnets were single-aperture quadrupoles or dipoles, whereas the common-coil design is for two-in-one dipoles. With the growing interest of the high-energy physics community in proton colliders with center-of-mass energies in the order of 100 TeV in a limited tunnel size (due to

geographic or other reasons), however, interest in a design option that can produce a lower cost high field magnet has returned (Qingjin Xu et al. 2016; Toral et al. 2017).

14.3.1 Optimization of Field Quality

Field quality in accelerator magnets is expressed in terms of the normal and skew harmonics (b_n and a_n) as defined in the expression

$$B_y + iB_x = B_1 \sum_{n=1}^{\infty} (b_n + ia_n) \left(\frac{x + iy}{R_{\text{ref}}} \right)^{n-1}$$

where B_x and B_y are the components of the field at (x, y), and B_1 is the magnitude of the field due to the most dominant harmonic at a "reference radius" R_{ref}. A reference radius of 10 mm is assumed for 40 mm aperture dipole designs and 17 mm for 50 mm aperture designs.

Field-quality design optimization in superconducting magnets is mostly associated with minimizing geometric and saturation-induced harmonics. The geometric and saturation-induced field harmonics are primarily optimized using the ROXIE software program (Russenschuck 1995).

Persistent-current induced harmonics, another source of errors, are primarily associated with the critical current density and the effective filament diameter of the conductor and the coil geometry. Due to the larger critical current density and typically larger filaments, the persistent-current induced harmonic errors are much larger in current high field conductors (Nb$_3$Sn, HTS) as compared to those in Nb-Ti composite wires.

All R&D common-coil magnets, except for the FNAL common-coil dipole (Ambrosio et al. 2000; Chap. 15, this book), built to date consisted of the main coil alone (see Fig. 14.1), and achieving a good field quality was not part of the initial considerations. A coil cross-section optimized for geometric harmonics of the level needed in accelerator magnets and minimizing the amount of conductor requires pole coil blocks (Gupta et al. 2000) or field-shaping coils. Type (a), as shown in Fig. 14.2a, uses a smaller amount of conductor but has more complicated ends than type (b), as shown in Fig. 14.2b, where all coils are flat racetrack coils but the conductor of the return side does not contribute to the main field. These additional coils add to the complexity of the magnet. The pole coils have to be designed such that they do not only provide good field quality, but are also well clamped within the structure and have sufficient margin.

Depending on the details of accelerator design, the dipole field created by the return conductors in type (b), which represents a small fraction of the overall conductor, can still be used for an injector (Gupta 1999); and therefore the conductor is efficiently used.

Fig. 14.2 Two possible
configurations of coil blocks
for good field quality: (**a**)
type (a) uses less conductor
but requires pole blocks
with flared ends to clear the
bore tube; contrary to (**b**)
type (b), where all of the
coils are flat
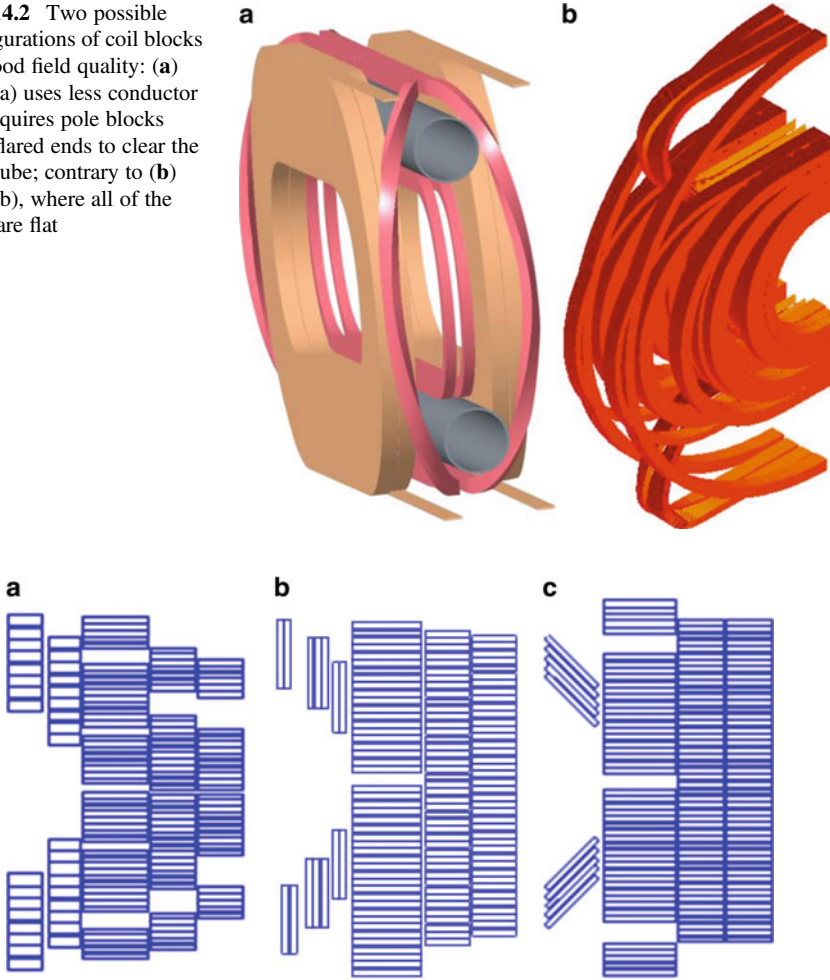
Fig. 14.3 Basic orientation of the pole coils: (**a**) horizontal; (**b**) vertical; and (**c**) inclined

Pole coils can be placed in one of three orientations: horizontal (the same as the main coil, see Fig. 14.3a), vertical (see Fig. 14.3b), and aligned (see Fig. 14.3c), or in combination (Gupta et al. 2000).

14.3.2 Example of an Optimized Common-Coil Dipole

A 50 mm aperture, 16 T common-coil dipole is presented here with the field quality optimized with the help of pole coils. The coil uses rectangular Nb_3Sn Rutherford

**Fig. 14.4** Optimized two-in-one common-coil dipole design
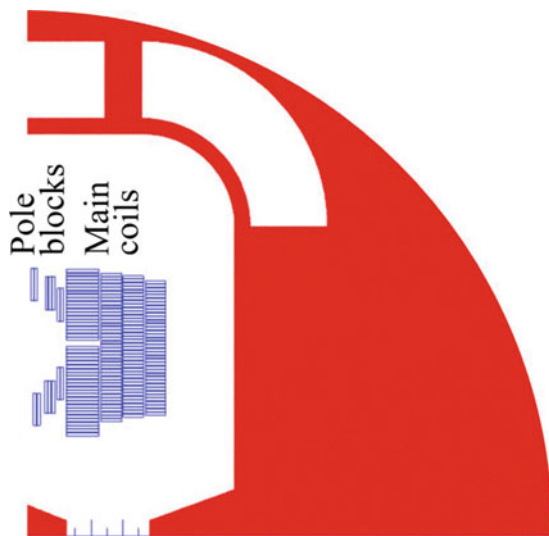
Table 14.1 Skew a_n and normal b_n harmonics at 17 mm radius at 16 T

a_2	a_4	a_6	a_8	a_{10}
0.00	0.00	0.00	0.27	0.21
b_3	b_5	b_7	b_9	b_{11}
0.00	0.00	0.01	−0.16	−0.10

cables with strands having a diameter of 1.1 mm and copper to non-copper ratios for the inner layer of 1.0 and for the outer layer of 1.5 (Toral et al. 2017). The critical current of the superconductor is 1500 A/mm^2 at 4.2 K and 16 T. The insulation thickness is 0.15 mm on either side. The number of strands in the inner layer and pole coils is 36 for a cable width of about 21.3 mm, and the number of strands in the outer three layers is 22 for a cable width of about 13 mm.

The optimized coil design (Gupta et al. 2017a) is shown in Fig. 14.4. It has less than 0.3% peak enhancement (maximum field on the conductor with respect to the field at the center of the bore). Computed harmonics for the design field of 16 T are given in Table 14.1 at a reference radius of 17 mm. Harmonics not listed in the table are zero by symmetry.

Harmonics having significant change as a function of current due to iron saturation are plotted in Fig. 14.5. Small saturation-induced harmonics were achieved ($b_3 <$ 7 units and $a_2 <$ 6 units). Enough space was also left (Gupta et al. 2017a) for the support structure. The fringe field at a radius of 150 mm outside the yoke is about 0.25 T when the yoke outer diameter (OD) is 700 mm (as in the design presented here), ~0.2 T when the yoke OD is 750 mm, and ~0.12 T when the yoke OD is 800 mm. Key parameters of the design are given in Table 14.2.
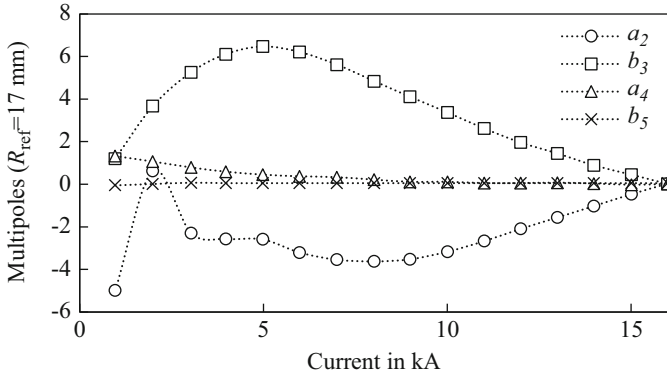
Fig. 14.5 Field harmonics at 17 mm reference radius vs. current

**Table 14.2** Key parameters of example design

Parameter	Value
Operating current (kA)	15.96
Field in the aperture (T)	16.0
Margin at 1.9 K (%)	19.3
Intra-beam spacing (mm)	250
Yoke outer diameter (mm)	700
Stored energy per unit length/aperture (MJ/m)	1.7
Inductance/aperture (mH/m)	13
Strand diameter (inner and pole layer) (mm)	1.1
Strands/cable (inner and pole layer)	36
Cu/non-Cu (inner and pole layer)	1.0
Strand diameter (outer layers) (mm)	1.1
Strands/cable (outer layers)	22
Cu/non-Cu (outer layers)	1.5
Total number of turns per aperture	179
Total area of Cu/aperture (mm^2)	5029
Total area of non-Cu/aperture (mm^2)	4026

14.3.3 Mechanical Analysis

To examine the basic issues related to the support structure, a simplified one-piece stainless-steel collar is assumed with no joints or connections. The coil modulus of fiberglass/epoxy impregnated Nb$_3$Sn is assumed to be 20 GPa. Symmetry (frictionless) is assumed at the horizontal split line and at the vertical split line. The thickness of the collar is 37 mm. A frictionless support is assumed on the right-hand edge of the collar.

Figure 14.6 shows the stresses on the coil powered to a field of 16 T at 1.9 K. The maximum stress on the main coil (Fig. 14.6a) is 144 MPa around the mid-plane of
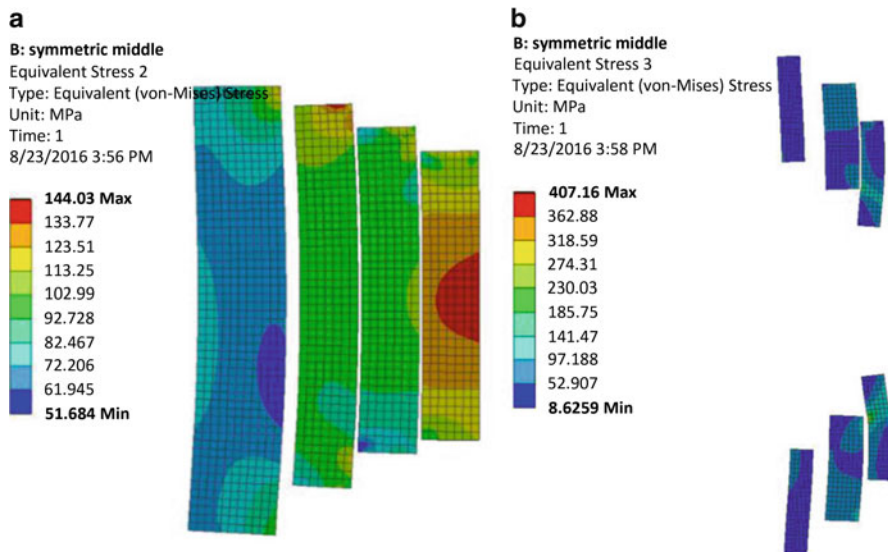
Fig. 14.6 Stresses (**a**) in the main coil; and (**b**) pole coils (MPa)

the outermost coil. This value remained about the same when collars were free to move with no support at the right edge. Stresses on the pole coils (Fig. 14.6b) are also generally below 150 MPa, except at the local area in the right-most pole coil blocks, where the stress is very high, above 400 MPa. This stress is to be reduced in future iterations of the structure.

Figure 14.7 shows the deflections in the main and pole coils under the Lorentz forces at 16 T. We plot the horizontal deflections for the main coil (Fig. 14.7a) and vertical deflections for the pole coil (Fig. 14.7b). The maximum horizontal deflection is about 0.77 mm (in the main coils). This deflection is considered acceptable if the coil moves as a whole (a major benefit of the common-coil design), so long as the relative deflections inside the coil are small to keep the strain within an acceptable limit. The horizontal deflection of the pole coil blocks will be limited by the main coils and the support structure. The goal of future iterations will be to make deflections more uniform. The vertical deflections are less than 0.1 mm, which indicates that the type of support structure considered for the pole coils should be able to hold them against the vertical Lorentz forces.

14.3.4 Influence of Coil Displacements on Field Harmonics

Deflections due to Lorentz forces have an impact on field harmonics, and their change might be significant when the deflections are as large as previously described. The change is expected to be small if deflections are more horizontal
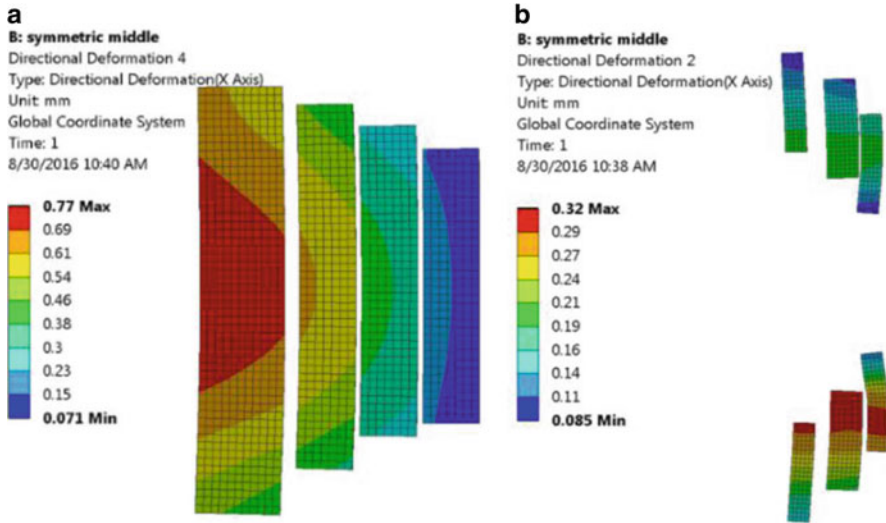
Fig. 14.7 (**a**) Horizontal displacements of the main coils; and (**b**) vertical displacement of the pole coils (mm)

rather than vertical, however, as is the case here. If all blocks are allowed to move horizontally, then a displacement of 1 mm primarily causes a change in the sextupole (b_3) harmonic. The impact is linear as a function of displacement and is computed to be about 9 units/mm. The field harmonics (in particular b_3) also change, however, due to iron saturation. Optimizing b_3 taking these two effects into account shows that its variation can be kept below 10 units from injection to collision energy.

14.4   BNL React-and-Wind Common-Coil Dipole DCC017

All so-far known practical high field superconductors are brittle. Nb_3Sn, however, offers the unique opportunity to wind the magnet with a strand containing the precursors (mainly Nb and Sn) and react the conductor after winding: an approach using W&R. On the other hand, the conductor can be reacted before winding, the R&W approach, which allows a variety of materials (including insulation) to be used since the coil and associated tooling are not subjected to high reaction temperatures.

Moreover, the I_c of Nb_3Sn degrades with strain in various background fields, as reported in Ekin (1980). It was found that I_c bending degradation is a function of strain and magnetic field, with a particularly large degradation at high fields above 10 T. Therefore, R&W high field magnet technology calls for magnetic designs with low bending strain, which has been a major challenge. For this reason, almost all high field Nb_3Sn short R&D accelerator magnets have been built using W&R technology.

Fig. 14.8 Schematic design
of the BNL dipole DCC017
with a pair of racetrack coils
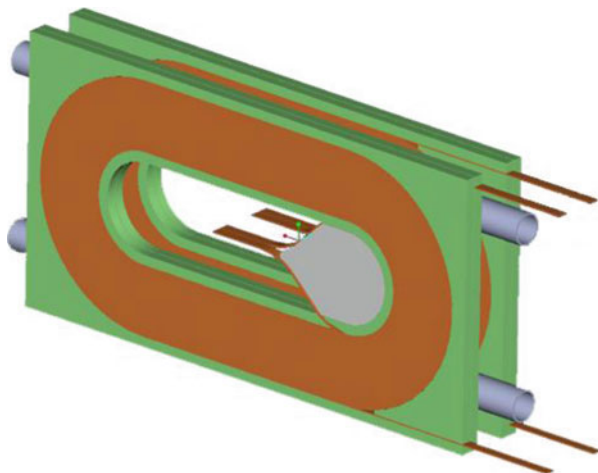
The 10.2 T dipole magnet developed by BNL (Ghosh et al. 1999; Escallier et al. 2001; Gupta et al. 2001, 2002; Cozzolino et al. 2003; Gupta 2015) and described in this chapter, is the highest field R&W Nb$_3$Sn accelerator R&D magnet ever built. Magnet design, construction, and test results are presented here. The successful construction and test of this magnet opens the possibility of using the R&W approach for longer magnets to be used in accelerators.

14.4.1 Magnet Design

The magnet is based on two pairs of flat racetrack coils (see Fig. 14.8) made with pre-reacted Nb$_3$Sn cable following the R&W approach. Stainless-steel collars in combination with a stainless-steel shell and an iron yoke contain the Lorentz forces. The coils are subjected to only minimal pre-stress in the horizontal, vertical, and axial directions at cold.

14.4.1.1 Magnetic Design

The magnetic design consisted of two coil layers in a two-in-one common-coil configuration (Gupta et al. 2007) with a minimum bending radius of 70 mm. The main parameters of the design are presented in Table 14.3. One quadrant of the magnet cross-section (one-half of one aperture) is shown in Fig. 14.9.

The bobbin (also known as the central island) on which the coil is wound was made of magnetic steel (the original design had a 5 mm non-magnetic liner). The use of magnetic steel reduces: (a) the peak field on the conductor; and (b) the loss in pre-stress from cool-down because of its lower thermal expansion as compared to

Table 14.3 Main parameters of common-coil dipole DCC017

Parameter	Value
Conductor type	Nb_3Sn
Magnet technology	React and wind
Horizontal coil aperture (clear space) (mm)	31
Vertical coil aperture (clear space) (mm)	338
Separation between apertures (mm)	220
Number of layers	2
Number of turns per quadrant (turns/layer)	45
Coil height (pole-to-pole) (mm)	85
Wire non-Cu J_{sc} (12 T, 4.2 K) (A/mm^2)	1900
Strand diameter (mm)	0.8
Number of strands in cable	30
Cable width (mm)	13.13
Cu/non-Cu ratio	1.53
Computed quench current (kA)	10.8
Computed quench bore field at 4.2 K (T)	10.2
Peak field at quench in inner layer/outer layer (T)	10.7/6.1
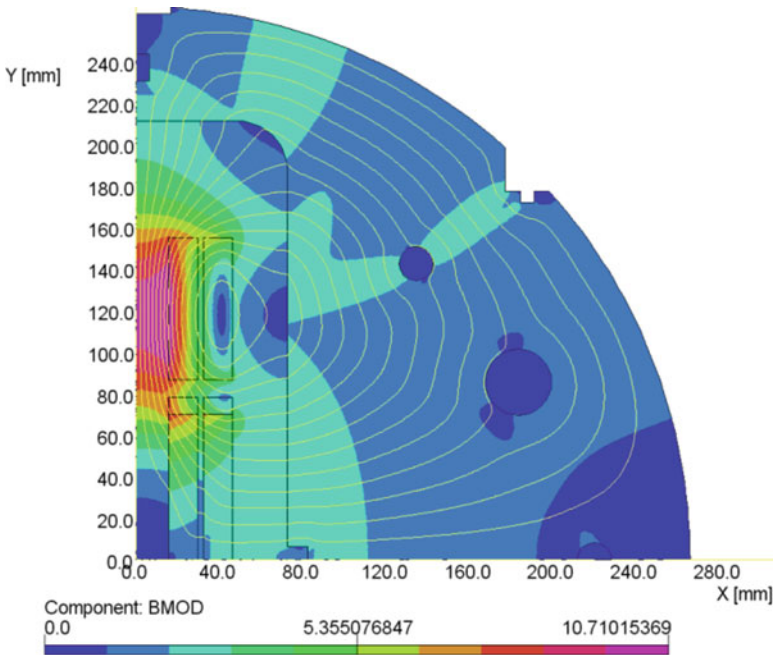
Fig. 14.9 A 2D model of one-quarter of the DCC017 common-coil dipole

Fig. 14.10 Overall
mechanical layout of
DCC017
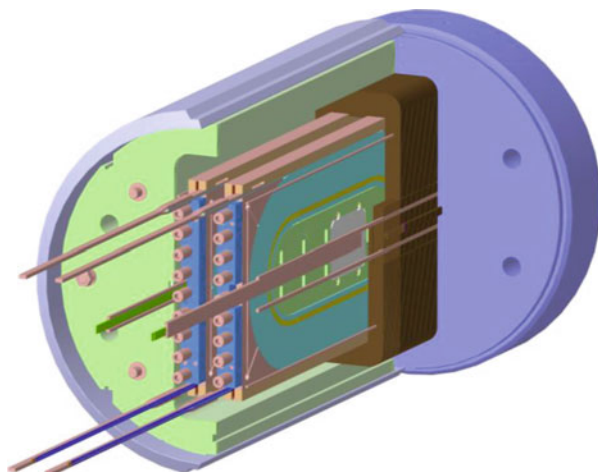
other materials (fiber-reinforced epoxy like G10, coil composite, copper) in the magnet structure.

In the cross-section of the common-coil magnet, the largest component of the Lorentz force is horizontal and is in the outward direction. The net vertical component of the Lorentz force on the entire coil (pole-to-pole) is small, while the conventional vertical stress on the mid-plane is about 35 MPa for one-quarter of the coil in one aperture. The direction of the vertical Lorentz force at low fields depends on the material of the bobbin. In the case of a non-magnetic bobbin the Lorentz forces are vertically outward or away from the bobbin; and in the case of a magnetic bobbin, they are towards the bobbin. In the present design, the computed horizontal/vertical components of the corresponding coil stresses in the first quadrant (right-hand side of the upper aperture of the magnet) are 43 MPa/−1.2 MPa at the computed quench field of 10.2 T, 59 MPa/−0.8 MPa at 12 T, and 77 MPa/−0.3 MPa at 13.8 T.

14.4.1.2 Mechanical Design

The overall mechanical structure of the magnet is shown in Fig. 14.10. The structure consists of 13 mm thick stainless-steel collars, and a rigid vertically split iron yoke having a radius of 267 mm, surrounded by a 25 mm thick welded stainless-steel shell. To restrict the movement of the ends, 127 mm stainless-steel end plates welded to the stainless-steel shell were used. Two 25 mm thick pusher plates, each equipped with nine bolts, were used on each magnet end to transfer coil end forces to the end plates (see Fig. 14.10). No pre-stress in the horizontal or vertical directions was envisaged in the coil's cross-sectional structural design. The screws were closed with minimal torque so as not to apply preload to the coil ends.

The end saddles and sidebars of the coils were made of stainless steel to keep the structure as rigid as possible. The brass spacer was slit at many places, which made it flexible so that its shape could more easily adapt to the layout of the cable in the ends and hence minimize the possibility of pinching the brittle cable. All coils were vacuum-impregnated individually with end saddles and sidebars installed.

To take full advantage of the modular nature of the common-coil design, all coil modules were deliberately made as identical single-layer mechanical cassettes with one splice in the middle so that their relative position in the R&D magnet could be interchanged (see Fig. 14.8). All coils had one 8.5 mm thick end spacer after five turns (counting from the inner radius, not shown in Fig. 14.9) to reduce the peak field in the ends. In addition, there was one wedge in the magnet cross-section that was also 8.5 mm thick and contiguous with the end spacer in the return end.

The guideline for this design was to keep the bending degradation in critical current below 15% to achieve a computed overall degradation of below 5%. Therefore, the bending strain had to be limited to around 0.3%, 0.25%, and 0.2% for 12 T, 14 T, and 15 T peak fields, respectively. Larger margins may, however, be available, as peak field and peak bending strain are not necessarily at the same location. In the design presented here, the peak bending strain is at the coil inner radius, and the peak field is at the coil mid-plane of either aperture.

As the field reduces over the coil width (see Fig. 14.9), the current density can be increased in coil layer 2 with respect to coil layer 1. This so-called grading can be achieved either by varying the cable area or by different currents in coil layers 1 and 2. A variable shunt power supply was introduced, which allowed grading of the current density in layer 1 and in layer 2. The shunt was incorporated in the construction of the magnet, but was never used. Therefore, the short sample field was reduced from the original design value of about 12 T to 10.2 T. The computed short sample limit of the magnet of 10.2 T is based on the actual configuration, cable measurements, and inclusion of the computed bending degradation (see Table 14.3).

The structure was designed to contain Lorentz forces at the original design field of 12 T in a 40 mm aperture. In this design, the horizontal component of the force was 75 MPa. Therefore, there is sufficient margin in the basic support structure, since the outward horizontal force in the present configuration at 10.2 T is only 59 MPa. The present mechanical structure can contain forces for fields up to 13.5 T.

Due to the large forces, the challenge in the common-coil design is to limit the displacement. A structural analysis, using ANSYS finite element software (ANSYS Inc., Canonsburg, PA), is shown in Fig. 14.11, which shows the deflections on the collar (Fig. 14.11a) and end plates (Fig. 14.11b). For a field of 13.5 T, the yoke vertical split remains in contact near the shell but opens 0.05 mm adjacent to the collar. The collars spread apart by 0.28 mm across the 44 mm aperture, but uniformity in the coil region is within 0.08 mm. The end plate deflects 0.41 mm under an axial force of 1.1 MN.

Fig. 14.11 ANSYS simulation showing stresses: (**a**) in the collar; and (**b**) on the end plates in the DCC017 common-coil dipole
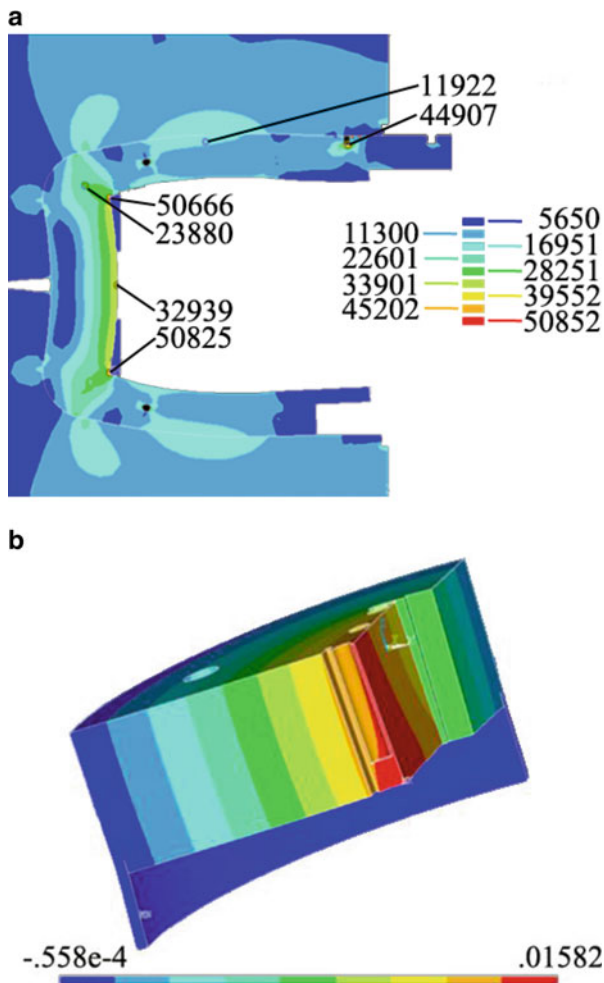
14.4.2   Strand and Cable

DCC017 used a 30-strand cable made from 0.8 mm diameter strand using the modified jellyroll process. The strand was manufactured by Oxford Instruments Superconducting Wire LLC ("OST"), which has been acquired by Bruker Energy and Supercon Technologies Inc ("BEST"), a subsidiary of Bruker Corporation (600 Milik Street, Carteret, NJ 07008, USA). The Nb₃Sn wire used came from two billets, ORE-163 and ORE-202. Both billets have the same nominal copper fraction of 60% (measured Cu/non-Cu ratio: ORE-163: 1.54 and ORE-202: 1.6).

Fig. 14.12 Vacuum-impregnation fixture for coating cable with Mobil-1® to avoid sintering

Coils for this magnet were made from two lengths of cable. Cable BNL-N-4-0012 was fabricated by New England Wire Company, 130 North Main Street, Lisbon, NH 03585 USA and cable BNL-6-O-B0899R was fabricated at LBNL. All cable lengths for the four coils were vacuum-impregnated (see fixture in Fig. 14.12) with Mobil-1®, and pre-annealed at 200 °C for 8 h to drive off the volatile constituents in the oil and to remove the strain in the copper. Mobil-1® from Exxon Mobil, 5959 Las Colinas Boulevard, Irving, Texas 75039-2298 USA was used to prevent sintering of the strands after reaction. To avoid sintering is important in a R&W magnet, because the strain degradation of bent sintered cables is larger by a factor of about two, as shown by experiments.

Four sections of cable about 130 m long were reacted in a vacuum furnace using the following heat treatment cycle: 48 h at 200 °C, 48 h at 400 °C, and 72 h at 665 °C. After reaction, the width and mid-thickness of cable BNL-N-4-0012 (used in coil 32) were 12.72 mm and 1.509 mm, respectively, and for cable BNL-6-O-B0899R (used in coils 33, 34, and 35) were 13.17 mm and 1.513 mm, respectively.

Extracted strands from the cable were reacted on stainless-steel barrels using the same reaction schedule as the cable segments. The critical current measurements of the extracted strands were carried out in the range 8–11.5 T, and fitted using Summers' formulation (Summers et al. 1991). Strand data are multiplied by 30 to calculate the cable I_c, as given in Table 14.4.

The cable was reacted on a 280 mm diameter stainless-steel drum. Therefore, after coil winding the bending strains experienced by the strand when: (a) the cable from the drum is straightened; and (b) the cable is bent at a radius of 70 mm, are similar in magnitude but opposite in sign. The effect of the bending is to add tensile strain along the outside of the strand and the same magnitude of compressive strain

**Table 14.4** Expected performance of cable used in DCC017

| B (T) | Cable critical current I_c (A) | | | |
| | Cable BNL-N-4-0012 (coil 32) | | Cable BNL-6-O-B0899R (coils 33, 34, and 35) | |
	Fitted	With strain	Fitted	With strain
9.0	19,710	16,077	21,348	17,458
9.5	17,970	14,383	19,404	15,687
10.0	16,260	12,838	17,618	14,068
10.5	14,649	11,427	15,975	12,587
11.0	13,188	10,137	14,462	11,230
11.5	11,820	8,959	13,065	9,986
12.0	10,650	7,882	11,776	8,847

along the inside of the strand. The magnitude of the bending strain is equal to r/R, where r is the radius of the filament boundary in the strand (0.58 mm diameter area in the 0.8 mm diameter strand) and R is the bending radius. Since the strand is reacted at a radius of 140 mm, the effective bending radius when the cable is bent at a radius of 70 mm is 140 mm (since the change in $1/R$ is $1/70 - 1/140 = 1/140$). From the as-reacted state, the strand J_c increases with tension and decreases with compression strain (Ekin 1980). Bending increases the compressive strain in the strand from the as-reacted state by $\Delta\varepsilon = 0.21\%$. The minimum I_c of the strand/cable is then calculated using Summers' fit (Summers et al. 1991) and changing the strain by $\Delta\varepsilon = -0.21\%$. In the absence of direct measurements, the calculated I_c sets a lower bound for the effect of bending strain. Since coil 32 is one of the inner coils and has the lowest performance, it will be the limiting coil when the magnet reaches the short sample limit. The calculated critical currents at 4.2 K and the strain-degraded current at 4.5 K are shown in Table 14.4. The category "Fitted" refers to the strand measurements at 4.2 K multiplied by the number of strands, 30, and the category "With strain" refers to the expected performance at 4.5 K in the magnet with a strain of $\varepsilon = -0.21\%$ due to bending, computed using Summers' formulation.

Figure 14.13 shows the magnet load lines and the critical current of the cable vs. magnetic field in coil 32 at a temperature of 4.5 K and a strain $\varepsilon = -0.21\%$. This gives a short sample limit of 10.8 kA using the computed peak field load line based on 2D and 3D models corresponding to a peak field of 10.7 T and a central field of 10.2 T in both apertures.

14.4.3 Tooling

Since pre-reacted Nb$_3$Sn conductor is brittle and sensitive to local strain, manual handling must be minimized to avoid accidental damage or degradation. The BNL coil winding tooling is shown in Fig. 14.14. Other major pieces of tooling developed for this program are the coil impregnation fixture using vacuum bag technology. One of the coils after impregnation is shown in Fig. 14.15.
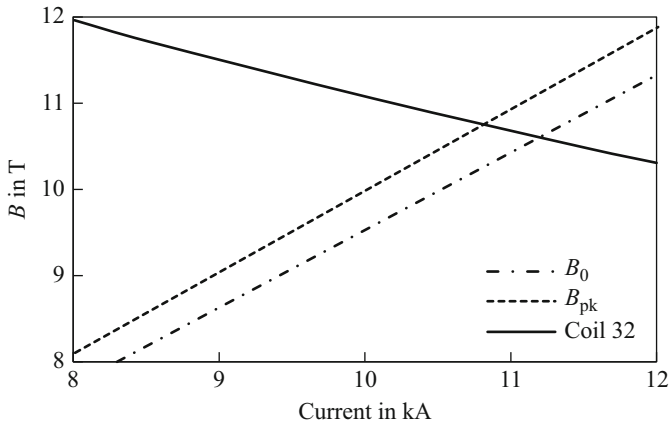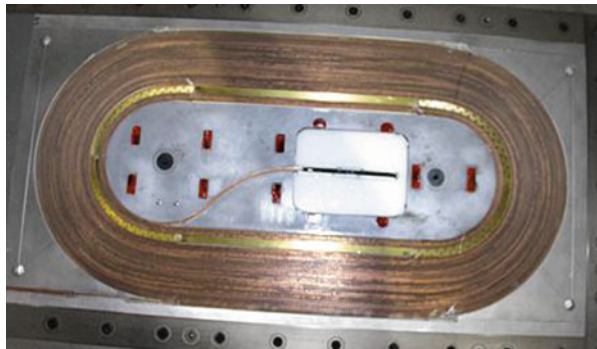
Fig. 14.13 Cable critical surface and DCC017 load lines: B_0 corresponds to the field in the aperture, B_{pk} corresponds to the maximum field in the coil

Fig. 14.14 Coil winding tooling

Fig. 14.15 Nb$_3$Sn coil after impregnation with CTD-101K epoxy (Composite Development Technology, Inc., 2600 Campus Drive, Lafayette, C0 80026, USA)

14.4.4 Magnet Construction

Four coils were wound with pre-reacted 30-strand Nb$_3$Sn cable on a magnetic steel flat racetrack bobbin having a straight section length of 300 mm and a bending radius of 70 mm. For the turn-to-turn insulation, 0.170 mm thick and 13.2 mm wide Nomex® tape (approximately the same width as the cable) was used. Nomex® is a trademark of DuPont, USA. Utmost care was taken to avoid over-straining the cable. The winding tension did not exceed 53 N for the cable and 67 N for the Nomex® tape. No clamps were used during winding. The cable freely followed its natural path from the straight section to the end, yielding to a negligible buckle. The thickness of the cable from edge to edge was slightly different, which caused a 7° inclination over the width of the 45th turn. No attempt was made to remove this condition due to concerns regarding possible conductor damage. After having finished winding, a minimal 222 N force was applied to straighten the straight section of the coil and to perform shimming against the bobbin. To compensate for the 7° inclination of the cable, tapered shims were used.

The end saddles and sidebars were made of stainless steel and were custom fit to each individual coil. No pre-compression was applied during coil impregnation and curing. All large voids were filled with fiberglass or G10. Each coil was checked for straightness and flatness after curing. The coils were pinned into pairs and shimmed to equal overall size with alumina-filled epoxy. Stainless-steel sheets having a thickness of 1.65 mm were placed between the layers of each coil pair to homogenize the stress distribution at full power. Four 0.025 mm thick stainless-steel strip heaters insulated with polyimide foil were placed on both sides of this sheet.

One of the two coil modules consisting of a pair of coils is shown in Fig. 14.16. This assembly contains an internal splice in a low-field region made with a set of 12 perpendicular Nb-Ti cables. A shunt lead (coming out axially in the middle) can

Fig. 14.16 Coil modules with a pair of coils and the shunt lead
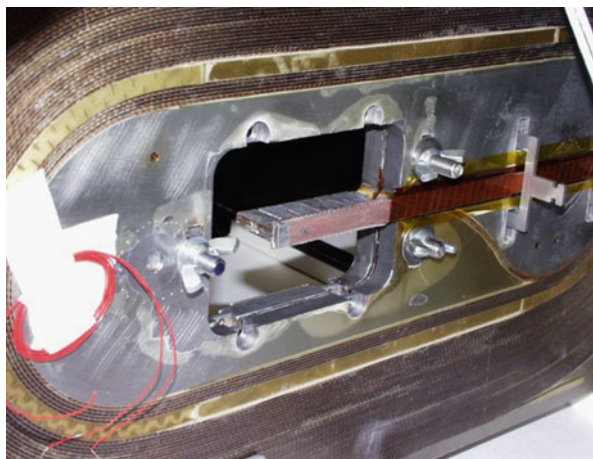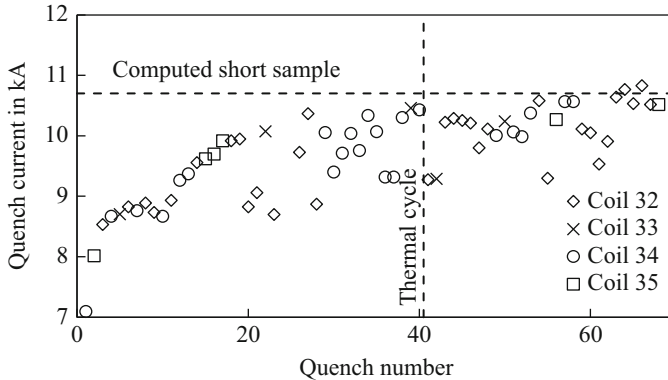
Fig. 14.17 DCC017 quench history. Short sample line at 10.8 kA corresponds to a peak field of 10.7 T and a bore field of 10.2 T

also be seen in Fig. 14.17. This shunt lead contains a Nb_3Sn cable since it passes through a high field region in the ends.

A collaring press was built specifically for this magnet. Coil pre-stress was strictly applied only in the side-to-side direction (cable stack direction) and was relatively low, around 17 MPa. An inflatable bladder was employed to keep the coils hard outward against the collars during collaring. Stainless-steel "keepers" were installed for locking the coils against the collars.

14.4.5   Magnet Test Setup and Test Procedure

The magnet was tested at the Vertical Test Facility at BNL in a liquid helium bath at a nominal temperature of 4.5 K. The magnet was instrumented with voltage taps located between the coils and at the leads to the coils so that the voltages of the four coils could be monitored during testing. Quenches were detected by monitoring the voltage difference between the coil pairs and generating a stop pulse when the voltage exceeded the threshold voltage level. An additional quench detection circuit used the difference between the total coil voltage and the current derivative voltage signal. No voltage taps in the body of the coils were installed.

Quench calculations, using the QUENCH software program (Wilson 1983), showed that coil "hot-spot" temperatures could exceed 400 K. At this temperature level, degradation of Nb_3Sn cable could start to develop due to thermo-mechanical strain effects. Calculations were performed to establish the relationship between the quench temperature and the quench integral quantity $\int I^2 \, dt$. It was decided to limit the quench temperature to 300 K where the quench integral limit was 21 $(kA)^2$ s.

Since energy extraction was not available for this test, the coils were instrumented with quench heaters. These consisted of two type 304 stainless-steel strips, each of

0.025 mm thickness and 38.1 mm width separated by 6.35 mm. They were installed between the layers in each coil pair and positioned along each side of the inside surfaces of each layer. The strips were mounted on both sides of the polyimide-wrapped stainless-steel sheet, which separated the layers of each coil pair and essentially prevented quench propagation between the layers. The quench heaters were connected into two circuits. Each circuit was equipped with its own power supply based on a capacitance of 21.7 mF, which provided 450 V and 105 A peak to quench the coils. The total insulation (polyimide with adhesive, fiberglass, and CTD-101K epoxy) was 1.07 mm thick between the heater strips and the bare conductor. There was no copper shunting provided on the stainless steel. Quench delay times at 4 kA after heater firing were measured at 100–200 ms due to the thermal diffusion barrier across the insulation.

Quench tests were performed by powering the magnet in the common-coil electrical configuration using a 30 kA, 15 V power supply. Current ramps were done at rates from 3 A/s to 200 A/s, with most quenches done at 25 A/s or less. On detection of a quench, a stop pulse from the quench detector shut off the power supply, fired the strip heaters, and triggered the fast data logger system to acquire voltage data at a 1 kHz sampling rate.

14.4.6   Test Results

A total of 66 quenches were done, of which 38 were performed before the thermal cycle. The initial training started at 7 kA and continued for 16 quenches up to almost 10 kA. Then, the quench behavior was erratic with quench currents spanning from 8699 A to 10,475 A. After the thermal cycle, the behavior was significantly less erratic, with most quench currents above 10 kA, reaching 10,846 A (10.2 T central field), a value slightly above the calculated short sample limit. Figure 14.17 shows the complete quench history, which included a thermal cycle and a ramp rate study at the end. The magnet was, as expected, mainly limited by coil 32, whose conductor had a slightly lower critical current density and reached its conductor limit before the other coils. The highest quench currents were achieved for 200 A/s ramp rates. No clear evidence for a ramp rate dependence could, however, be found.

The training and erratic quenches occurred in all four coils. Measurements of the initial slope of the voltage increase gave values of dV/dt that varied from 6 V/s to 100 V/s and showed no correlation with the quench current, with different values of dV/dt resulting from similar quench currents, implying that locations within the coils varied. Pre-quench voltage spike detection was limited to a resolution of 60 mV and 1 ms. Most quench signals exhibited voltage spikes, some of which were recognized as flux jump instabilities. The voltage spikes ($\geq$60 mV) were, however, typically not at quench onset. Few quenches exhibited spikes right at quench onset above 60 mV.

Starting with quench number 46, the delay between the quench detector stop pulse and power supply shutoff/strip heater trigger was reduced from 58 ms to 16 ms by inhibiting the power supply firing circuit. The delay was minimized to decrease

the amount of heating in the coils after each quench. The quench integral was often above 16 $(kA)^2$ s, with a maximum of 19.1 $(kA)^2$ s. These values corresponded to a quench temperature of about 220 K, which was well below the safe limit of 300 K.

In February 2017, after a 10-year hiatus, DCC017 was recommissioned to test a HTS insert coil (Gupta et al. 2017b). The magnet performed flawlessly, reaching 92% of short sample field without quenching. A limitation of the leads, not the magnet itself, prohibited powering it to higher currents.

14.5   Magnet R&D Approach

The third purpose of building DCC017 was to commission an R&D superconducting coil test facility, which allows racetrack coils to be inserted and tested in the background field magnet of this magnet. This facility will, in principle, allow coils to be tested in a manner in which, previously, only cables have been tested. The DCC017 magnet was specifically designed with a large opening (31 mm wide and 338 mm high) where new R&D coils (HTS or Nb_3Sn) can be inserted and tested together with the existing background field Nb_3Sn coils (see Fig. 14.18). The most appealing part of this powerful magnet facility is that coil testing requires no disassembling of the background field magnet, facilitating a new way of doing "rapid turn-around" and "low-cost" magnet R&D. Another major motivation pursued within this program is to facilitate integration of the field-shaping pole coil in DCC017 to demonstrate a proof-of-principle common-coil dipole.

Fig. 14.18 End view of 10 T Nb_3Sn common-coil dipole DCC017 with a large open space
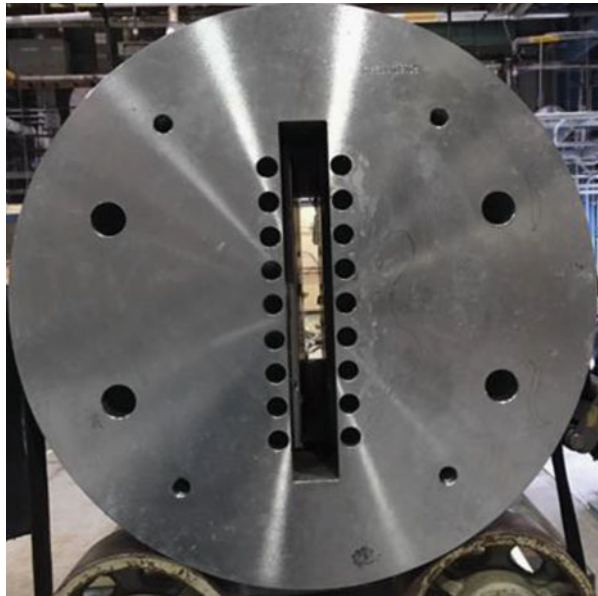
14.6 Conclusion

The common-coil design offers several inherent technical and cost advantages. It is suitable for high field magnets where the Lorentz forces are large. Simple geometry offers lower cost manufacturing options. Moreover, it also allows the use of R&W technology, as successfully demonstrated in the BNL Nb$_3$Sn DCC017 magnet.

DCC017 has been commissioned as a unique vehicle for carrying out low-cost, rapid turn-around magnet R&D. The DCC017 magnet has been found to be very robust, as it reached 92% of short sample without quench after a decade of hibernation.

Several designs have been developed, which show that the common-coil design can produce magnets with the field quality needed in accelerator magnets. The proof of the principle of high field magnets of accelerator quality based on this concept is yet awaited.

References

Ambrosio G, Andreev N, Barzi E et al (2000) Study of the react and wind technique for a Nb$_3$Sn common coil dipole. IEEE Trans Appl Supercond 10(1):338–341. https://doi.org/10.1109/77.828243

Cozzolino J, Anerella M, Escallier J et al (2003) Magnet engineering and test results of the high field magnet R&D program at BNL. IEEE Trans Appl Supercond 13(2):1347–1350. https://doi.org/10.1109/tasc.2003.812665

Danby G, Palmer R, Huson R et al (1983) Panel discussion of magnets for a big machine. In: Cole TF (ed) Proceedings of the 12th international conference on high energy, Fermilab, 11–16 Aug 1983. Fermilab, Batavia, pp 52–62

Ekin JW (1980) Strain scaling law for flux pinning in practical superconductors. Part 1: basic relationship and application to Nb$_3$Sn conductors. Cryogenics 20(11):611–624. https://doi.org/10.1016/0011-2275(80)90191-5

Escallier J, Anerella M, Cozzolino J et al (2001) Technology development for react and wind common coil magnets. In: Lucas P, Webber S (eds) Proceedings of the 2001 particle accelerator conference PAC2001, Chicago, 18–22 June 2001, vol 1. IEEE, Piscataway, pp 214–216

Fermilab (2001) Design study for a staged Very Large Hadron Collider. Fermilab TM-2149, 4 June, http://lss.fnal.gov/archive/test-tm/2000/fermilab-tm-2149.pdf

Ghosh AK, Cozzolino JP, Harrison MA et al (1999) A common coil magnet for testing high field superconductors. In: Luccio A, MacKay W (eds) Proceedings of the 1999 particle accelerator conference, New York, 27 Mar–2 Apr 1999, vol 5. IEEE, Piscataway, pp 3230–3232

Gupta G (1997) A common coil design for high field 2-in-1 accelerator magnets. In: Comyn M, Craddock MK, Reiser M et al (eds) Proceedings of the 1997 particle accelerator conference, Vancouver, 1997. IEEE, Piscataway, pp 3344–3346

Gupta R (1999) Common coil magnet system for VLHC. In: Luccio A, MacKay W (eds) Proceedings of the 1999 particle accelerator conference, New York, 27 Mar–2 Apr 1999, vol 5. IEEE, Piscataway, pp 3239–3241

Gupta R (2015) Common coil magnet design for high energy colliders (talk). In: CERN MSC seminar, 15 Sep, Todesco E (chair). https://indico.cern.ch/event/442002/

Gupta R, Chow K, Dietderich D et al (1999) A high field magnet design for a future hadron collider. IEEE Trans Appl Supercond 9(2):701–704. https://doi.org/10.1109/77.783392

Gupta R, Ramberger S, Russenschuck S (2000) Field quality optimization in a common coil magnet design. IEEE Trans Appl Supercond 10(1):326–329. https://doi.org/10.1109/77.828240

Gupta R, Anerella M, Cozzolino J et al (2001) Common coil magnet program at BNL. IEEE Trans Appl Supercond 11(1):2168–2171. https://doi.org/10.1109/77.920287

Gupta R, Anerella M, Cozzolino J et al (2002) R & D for accelerator magnets with react and wind high temperature superconductors. IEEE Trans Appl Supercond 12(1):75–80. https://doi.org/10.1109/tasc.2002.1018355

Gupta R, Anerella M, Cozzolino J et al (2007) React and wind Nb_3Sn common coil dipole. IEEE Trans Appl Supercond 17(2):1130–1135. https://doi.org/10.1109/tasc.2007.898139

Gupta R, Anerella M, Cozzolino J et al (2017a) Common coil dipoles for future high energy colliders. IEEE Trans Appl Supercond 27(4):1–5. https://doi.org/10.1109/tasc.2016.2636138

Gupta R, Anerella M, Cozzolino J et al (2017b) Design, construction, and test of HTS/LTS hybrid dipole. IEEE Trans Appl Supercond 28(3):1–5. https://doi.org/10.1109/tasc.2017.2787148

Russenschuck S (1995) A computer program for the design of superconducting accelerator magnets. In: 11th annual review of progress in applied computational electromagnetics, Monterey, CA, 20–24 Mar 1995, CERN AT/95-39, vol 1, pp 366–377

Sabbi G, Ambrosio G, Andreev N et al (2000) Conceptual design of a common coil dipole for VLHC. IEEE Trans Appl Supercond 10(1):330–333. https://doi.org/10.1109/77.828241

Summers LT, Guinan MW, Miller JR et al (1991) A model for the prediction of Nb_3Sn critical current as a function of field, temperature, strain and radiation damage. IEEE Trans Magn 27 (2):2041–2044. https://doi.org/10.1109/20.133608

Tommasini D, Auchmann B, Bajas H et al (2017) The 16 T dipole development program for FCC. IEEE Trans Appl Supercond 27(4):4000405. https://doi.org/10.1109/TASC.2016.2634600

Toral F, García-Tabarés L, Martinez T et al (2017) The EuroCirCol 16 T common-coil dipole option for the FCC. IEEE Trans Appl Supercond 27(4):1–5. https://doi.org/10.1109/tasc.2016.2641483

Wang C, Zhang K, Xu Q (2016) R&D steps of a 12-T common coil dipole magnet for SPPC pre-study. Int J Mod Phys A 31(33):1644018. https://doi.org/10.1142/s0217751x16440188

Wilson M (1983) Superconducting magnets. Clarendon Press, Oxford

Xu Q, Zhang K, Wang C et al (2016) 20-T dipole magnet with common-coil configuration: main characteristics and challenges. IEEE Trans Appl Supercond 26(4):1–4. https://doi.org/10.1109/tasc.2015.2511927